



CrossMark  
click for updates

Cite this: *Environ. Sci.: Processes Impacts*, 2015, 17, 1386

## Physicochemical and ion-binding properties of highly aliphatic humic substances extracted from deep sedimentary groundwater†

Takumi Saito,<sup>\*ab</sup> Motoki Terashima,<sup>c</sup> Noboru Aoyagi,<sup>d</sup> Seiya Nagao,<sup>e</sup> Nobuhide Fujitake<sup>f</sup> and Toshihiko Ohnuki<sup>b</sup>

Humic substances (HSs) are ubiquitous in various aquatic systems and play important roles in many geochemical processes. There is increasing evidence of the presence of HSs in deep groundwater; nevertheless, their ion binding properties are largely unknown. In this study we investigated the physicochemical and ion-binding properties of humic and fulvic acids extracted from deep sedimentary groundwater. The binding isotherms of protons (H<sup>+</sup>) and copper (Cu<sup>2+</sup>) were measured by potentiometry and fitted to the NICA-Donnan model, and the obtained parameters were compared with the generic parameters of the model, which are the average parameters for HSs from surface environments. The deep groundwater HSs were different from surface HSs, having high aliphaticities, high sulfur contents, and small molecular sizes. Their amounts of acidic functional groups were comparable to or slightly larger than those of surface HSs; however, the magnitude of Cu<sup>2+</sup> binding to the deep groundwater HSs was smaller. The NICA-Donnan model attributed this to the binding of Cu<sup>2+</sup> to chemically homogeneous low affinity sites, which presumably consist of carboxylic groups, via mono-dentate coordination at relatively low pH. The binding mode tended to shift to multi-dentate coordination with carboxylic groups and more heterogeneous alcoholic/phenolic groups at higher pH. X-ray absorption spectroscopy also revealed that Cu<sup>2+</sup> binds to O/N containing functional groups and to a lesser extent S containing functional groups as its divalent form. This study shows the particularity of the deep groundwater HSs in terms of their physicochemical and ion-binding properties, compared with surface HSs.

Received 17th April 2015  
Accepted 2nd July 2015

DOI: 10.1039/c5em00176e

rsc.li/process-impacts

### Environmental impact

For future use of deep underground space it is necessary to monitor and protect the quality of deep groundwater. Development of mechanistic models that can describe reactions of pollutants with components in groundwater is mandatory, as is the case for surface water systems. Humic substances (HSs) play important roles in the speciation of metal ions; nevertheless, the details of ion binding to deep groundwater HSs are largely unknown. This study reveals the particularity of the physicochemical and ion-binding properties of the HSs extracted from sedimentary groundwater by comparing them to those of surface HSs.

## 1. Introduction

Humic substances (HSs) are a class of natural organic matter resulting from the degradation and condensation of animal, plant and microbial remains, and are ubiquitous in various environments: surface and ground water, ocean, soil, and the atmosphere.<sup>1,2</sup> A HS is not a molecular entity with a distinct structure, but should be considered as a group of organic molecules with certain physicochemical properties in common.<sup>3</sup> Based on the solubility to water at different pH values, they are operationally divided into humic acid (HA), which is soluble at pH > 2, fulvic acid (FA), which is soluble at both acidic and alkaline pH, and insoluble humin. HSs play important roles in various environmentally-relevant processes; they determine structures of micro aggregates in soils,<sup>3</sup> stabilize

<sup>a</sup>Nuclear Professional School, School of Engineering, The University of Tokyo, 2-22 Shirakata Shirane, Tokai-mura, Ibaraki, 319-1188, Japan. E-mail: saito.takumi@jaea.go.jp; takumi.saito@nuclear.jp; Fax: +81-29-282-5927; Tel: +81-29-284-3518

<sup>b</sup>Advanced Science Research Center, Japan Atomic Energy Agency (JAEA), 2-4 Shirakata, Tokai-mura, Ibaraki, 319-1195, Japan

<sup>c</sup>Radioactive Waste Processing and Disposal Research Department, JAEA, 4-33 Muramatsu, Tokai-mura, Ibaraki, 319-1194, Japan

<sup>d</sup>Nuclear Science and Engineering Center, JAEA, 2-4 Shirakata, Tokai-mura, Ibaraki, 319-1195, Japan

<sup>e</sup>Institute of Natural and Environmental Technology, Kanazawa University, Wake, Nomi, Ishikawa 923-1224, Japan

<sup>f</sup>Graduate School of Agricultural Science, Kobe University, Rokkodai1, Kobe 657-8501, Japan

† Electronic supplementary information (ESI) available. See DOI: 10.1039/c5em00176e



metastable minerals,<sup>4</sup> catalyze redox reactions,<sup>5</sup> and capture inorganic and organic contaminants.<sup>6–8</sup> Protons and metal ions readily bind to the functional groups of HSSs,<sup>8,9</sup> mostly carboxylic and phenolic groups and less significantly amine and sulfur-containing groups, and alter their reactivity, bioavailability, and mobility.<sup>7,10</sup>

Ion binding to HSSs has been an active topic of research for decades.<sup>11–13</sup> The particularity of HSSs as ligands lies in their chemical heterogeneity and polyelectrolyte nature.<sup>9,13</sup> The former is manifested in the distribution of the affinity constant of a HS for a given metal ion due to the diversity of the environments surrounding its functional groups. The latter originates from negative charges located on its carbon backbone, which creates a negative electrostatic potential that attracts cations and excludes anions.<sup>14,15</sup> Recent mechanistic models for ion binding to HSSs such as the NICA-Donnan model<sup>9,11</sup> and the Model VI and its successor<sup>12,16</sup> take these aspects into account and can successfully describe the binding of various cations over a wide range of conditions. These models have been well tested for HSSs extracted from different surface environments.<sup>12,17,18</sup> There are certain similarities in the obtained model parameters, once HAs and FAs are separately discussed.<sup>17</sup> Thus, so-called “generic” parameters have been proposed for these two groups of HSSs<sup>12,17,18</sup> and are widely used to estimate the level of metal binding to HSSs for which specific model parameters are unavailable.<sup>19,20</sup>

There is increasing evidence showing the presence of HSSs in deep underground environments either as dissolved forms in pore water or bound to host rocks.<sup>21–29</sup> Deep underground environments are rather different from surface aquatic systems, as manifested by slow groundwater flow, which leads to prolonged interaction between rocks and dissolved/suspended components, low oxygen concentration, and no direct energy input from the sun. It is likely that HSSs in deep underground environments are different from their counterparts in surface environments with respect to their structures and ion binding properties.<sup>21,23</sup> Underground HSSs may originate from surface waters transported by downward recharge, dissolution of sedimentary organic materials, or *in situ* production from the remains of microorganisms or algae in connate water, and have experienced long-term diagenesis. Ratios of dissolved and bound HSSs in deep underground environments are different from site to site, and they may have rather different properties even in a given geological setting.<sup>30</sup>

The uniqueness of deep underground HSSs has been pointed out by several researchers.<sup>21,23–26,29,31,32</sup> Schäfer *et al.*<sup>23</sup> studied possible sources of FAs in the Gorleben aquifer, based on isotopic data and C and S X-ray absorption near-edge spectroscopy (XANES). They reported that FAs derived from the deep brine groundwater at around –216 m below ground level (bgl) had similar carbon backbone structures to those of FA in the corresponding shallow recharge groundwater and that HAs and FAs originated from lignite in Miocene sediments were highly aromatic. Alberts *et al.*<sup>32</sup> reported that the properties of HA and FA extracted from groundwater at –30 to –70 m bgl were different from those of their counterparts from surface water, but copper binding to them was similar.

Courdouan *et al.*<sup>30</sup> studied the binding of trivalent metal ions to extracts of organic matter from pore water and rocks in the Opalinus clay (OPA) and the Callovo-Oxfordian formations and found stronger binding of curium to pore-water organic matter from OPA. Although some properties of deep underground HSSs such as elemental composition, <sup>13</sup>C NMR carbon distribution, optical properties, and molecular-size distribution have been reported,<sup>21,24–26</sup> their ion binding properties over a wide range of conditions remain largely unknown.<sup>31–33</sup> This is particularly the case for deep groundwater HSSs, as large-scale extraction of HSSs from deep groundwater is limited.

Deep groundwater HSSs can be extracted from pumped groundwater, using boreholes from the surface. Some countries are operating underground research laboratories (URLs) for feasibility tests of geological disposal of nuclear wastes, where large amounts of groundwater samples are available with less contamination or alteration.<sup>34–37</sup> This makes URLs appropriate places for extraction of deep groundwater HSSs.

Considering the future uses of deep underground space by mankind such as geological disposal of nuclear wastes and potential deterioration of groundwater quality, the ion binding properties of deep groundwater HSSs are to be studied and the applicability of the aforementioned mechanistic models is to be tested, as is the case for surface HSSs. Thus, the objective of this study is to reveal the physicochemical and ion-binding properties of HA and FA isolated from sedimentary groundwater at the Horonobe URL of the Japan Atomic Energy Agency (JAEA).<sup>35</sup> The physicochemical properties of the Horonobe HSSs, which are denoted as HHSSs hereafter, were compared with those of surface HAs and FAs to discuss their structural differences. Binding isotherms of protons (H<sup>+</sup>) and copper (Cu<sup>2+</sup>) were measured over a wide range of conditions by potentiometric titration and fitted to the NICA-Donnan model.<sup>9,11</sup> The results were compared to the model calculations with the generic parameters proposed by Milne *et al.*,<sup>18</sup> which capture average trends of ion binding to HSSs from surface environments. The oxidation state and local coordination environment of Cu<sup>2+</sup> bound to the HA fraction of the HHSSs were also assessed by X-ray absorption spectroscopy (XAS). Copper was chosen as a representative divalent metal ion in this study to examine the general metal binding properties of the HHSSs, as it can be easily quantified by an ion selective electrode (ISE) and its binding to surface HSSs has been well studied.<sup>18,38,39</sup> Copper is also an essential trace element for organisms at low concentration and becomes toxic at elevated concentrations.<sup>40,41</sup> It could be introduced to deep groundwater systems by exploitation of underground space, as it is an important constituent of various materials used in modern industries. Thus, studies on the speciation Cu<sup>2+</sup> in the presence of groundwater HSSs are relevant for its fate in deep groundwater environments. Although the HA and FA from a single groundwater source are examined in this study, the outcomes can be applied or be a good starting point to estimate the degree of metal binding to HSSs in sedimentary groundwater similar to this study.



## 2. Materials and methods

### 2.1. Materials

For all experiments, Milli-Q grade pure water and analytical-grade chemicals purchased from Wako Pure Chemical Industries were used, unless otherwise noted.

HA and FA were extracted from groundwater collected at the –250 m gallery of the Horonobe URL located in the northern part of Hokkaido Prefecture, Japan. The geology and geochemistry of the site are described elsewhere.<sup>35,42</sup> The –250 m gallery is located at the boundary of the Pliocene Koetoi and the Miocene Wakkanai formations, which are composed of diatomaceous and siliceous mudstones, respectively. Groundwater at the sampling location is a weakly alkaline  $\text{Na}^+/\text{HCO}_3^-$  type with relatively high total organic carbon (TOC) and  $\text{Cl}^-$  levels. Groundwater after filtration and acidification was passed through a column packed with DAX-8 resins (Supelite DAX-8, Sigma-Aldrich). Separation and extraction of HA and FA fractions from the loaded resins and subsequent purification was performed in a laboratory on the surface, according to the protocol recommended by the International Humic Substances Society (IHSS).<sup>43</sup> In total 6.6 g of HA and 3.5 g of FA were obtained by treating approximately 6000 L of the groundwater. These values correspond to approximately 8.5 and 4.5% of the TOC in the groundwater, respectively. Hereafter, the HA and FA fractions are denoted as HHA and HFA, respectively.

### 2.2. Characterization of HSSs

Elemental compositions and  $^{13}\text{C}$  NMR carbon distributions of the HHSs were evaluated in the same manner as a previous report.<sup>33</sup> Carbon, H and N contents were determined using an elemental analyzer (Yanagimoto, MT-6), and that of S was analyzed by ion chromatography after conversion to  $\text{SO}_4^{2-}$ . Ash contents were also determined by combustion at 550 °C. For  $^{13}\text{C}$  NMR a 50 mg HS sample was dissolved in a mixture of 0.02 mL of 10 M NaOD (99.9% deuteration, Sigma-Aldrich) and 0.4 mL of  $\text{D}_2\text{O}$  (99.9% deuteration, Sigma-Aldrich) solution. As a reference material for the chemical shifts, 0.02 mL of a 1.0% solution of sodium 3-trimethylsilylpropionate-2,2,3,3- $\text{D}_4$  (TMSP; 98% deuteration, French Atomic Energy Commission, CEA) was added into the mixture. The test solution was then passed through a glass-fiber filter with a pore size of 0.7  $\mu\text{m}$ , and placed in a 5 mm diameter spin tube.  $^{13}\text{C}$  NMR spectra were recorded by a Bruker AVANCE 500 spectrometer operating at 125.77 MHz. The inverse gated decoupling technique was applied for the measurement with a pulse width of 45° and acquisition time of 0.839 s. A total repetition time of 2.5 s was applied to permit relaxation of all the spins, and 4000–20 000 scans were accumulated. Chemical shift assignments were made using data reported by Wilson<sup>44</sup> and Fujitake and Kawahigashi.<sup>45</sup>

The UV/Vis absorption spectra of the HHS as well as those of the standard or reference HSSs from the international humic substances society (IHSS) and the Japanese humic substance society (JHSS) and purified Aldrich HA (PAHA)<sup>46</sup> were measured in this study by a UV/Vis spectrometer (UV-3100, Shimadzu). The samples were prepared as 50 mg  $\text{L}^{-1}$  HS solutions in 0.01 M

$\text{NaHCO}_3$  buffer.<sup>47</sup> The size distributions of HHA and HFA were determined by flow-field flow fractionation (FI-FFF) with 1 kDa polyethersulfone membrane (AF2000, Postnova), according to Lukman *et al.*<sup>48</sup> The electron accepting capacities (EAC) of the HHS and the standard HSSs from the IHSS and JHSS were determined by the mediator electrochemical reduction (MER) in a similar way to Aeschbacher *et al.*,<sup>49</sup> using diquat dibromide monohydrate (99.5%, Supelco) as a mediator. The details of the MER measurement are given in the ESI.†

### 2.3. Potentiometric titration

Potentiometric titration of HHA and HFA was performed using the Wallingford titration system.<sup>50</sup> HHS solutions were prepared by dissolving the freeze-dried samples in alkaline solutions at around pH 9 and kept stirred overnight.<sup>51</sup> The pH and  $\text{Cu}^{2+}$  activities were measured by a glass electrode (Metrohm, 6.0150.100) and a Cu ISE (Metrohm, 6.0502.140), combined with a 3 M KCl Ag/AgCl reference electrode (Metrohm, 6.0733.100) in an electrolyte bridge (0.1 M  $\text{NaClO}_4$ , Schott B511). All titrations were performed in a thermostated vessel under a slight over-pressure of moisturized Ar and continuous stirring. The glass electrode was calibrated by titrating  $\text{HClO}_4$  solutions with 0.1 M NaOH. The Cu ISE was calibrated by titrating 0.36 mM  $\text{Cu}(\text{ClO}_4)_2$  solution with 0.02 M ethylenediamine solution (Aldrich). The electrode calibrations were performed at the same salt levels as those in the subsequent sample titrations.

Proton binding isotherms of the HHSs were obtained by acid–base titration, as described elsewhere.<sup>46</sup> 30 mL of a 1 g  $\text{L}^{-1}$  HHA or HFA solution was first titrated to pH 4 and stirred for 1 hour; then three-sets of forward and backward titrations were performed. The salt concentration of the solution was increased by adding a 1 M  $\text{NaClO}_4$  solution (Merck) between the different sets of titrations. At every point of the titration the reading of the glass electrode was recorded when the drift became less than 0.1 mV  $\text{min}^{-1}$  or after 30 min. The relative positions of the charge ( $-q$ )–pH curves of the HHSs at the different salt levels were determined from the amounts of base and acid titrants necessary to back-titrate  $\text{H}^+$  released in the pH-stat salt titration. The absolute position of the curves was then determined by optimizing the initial negative charge,  $q_0$ , at the beginning of the titration in the NICA-Donnan fitting,<sup>11</sup> as described in the ESI.† The results of the forward base titration were used in the subsequent fitting, as the hysteresis between the forward and backward titrations at a given salt level was small. The uncertainty in the determination of the HHS charge,  $q$ , was estimated to be less than 0.1 meq  $\text{g}^{-1}$ , using a typical standard deviation of the glass electrode calibration (0.05 pH unit).

Copper binding isotherms to the HHSs were measured by pH-stat titration at three pH levels (pH 4, 6, and 8) and 0.1 M  $\text{NaClO}_4$ .<sup>38</sup> At pH 4 the additional titration of 0.01 M  $\text{NaClO}_4$  was performed. The  $\text{Cu}^{2+}$  titration to HFA at pH 8 failed most likely because of poor pH buffering (see the discussion below). 30 mL of a 1 g  $\text{L}^{-1}$  HHA or HFA solution was first titrated to pH 4 and stirred for 1 hour, and then to a desired pH and equilibrated within 0.2 mV (0.003 pH unit) for 30 min. After equilibration a



0.1 M  $\text{Cu}(\text{ClO}_4)_2$  solution or  $10^{-3}$  M  $\text{Cu}(\text{ClO}_4)_2$  solution in 0.1 M  $\text{NaClO}_4$  was added. The pH of the sample solution was back-titrated to the original value and kept within 0.2 mV for 20 min by addition of the acid and base titrants. Readings of the electrodes were recorded after their drifts became less than 0.1 mV  $\text{min}^{-1}$  or after 20 min. At each titration point the solution was checked for the formation of  $\text{Cu}(\text{OH})_2(\text{s})$  ( $\log K_{\text{sp}} = -19.32$  (ref. 52)) and the  $\text{Cu}^{2+}$  binding amount ( $[\text{Cu}^{2+}]_{\text{bound}}$ ) was calculated by subtracting the sum of the concentrations of free  $\text{Cu}^{2+}$  and its hydrolysis products from the total concentration, using the hydrolysis constants of  $\text{Cu}^{2+}$ .<sup>52</sup> The magnitude of the uncertainty in  $\log[\text{Cu}^{2+}]_{\text{bound}}$  was estimated to be no more than 0.2, using a typical error of the Cu ISE calibration (0.06 as the logarithm of  $\text{Cu}^{2+}$  activity,  $\log a_{\text{Cu}}$ ).

The obtained  $\text{H}^+$  and  $\text{Cu}^{2+}$  binding isotherms to HHA and HFA were fit to the NICA-Donnan model,<sup>9,11</sup> using an in-house MATLAB® program. The details of the model as well as the fitting procedure are given in the ESI†. First, the maximum density of  $\text{H}^+$  binding sites,  $Q_{\text{max},j,\text{H}}$  of the site  $j$  ( $j = 1$  and  $2$  for the low-affinity and high-affinity sites, respectively), the median values of the affinity constants of the site  $j$  for  $\text{H}^+$ ,  $\tilde{K}_{j,\text{H}}$ , the apparent heterogeneity parameters of the site  $j$ ,  $m_j$ , the Donnan parameter,  $b$ , and  $q_0$  were optimized, using the charge/pH curves. Then, the median values of the affinity constants of the site  $j$  for  $\text{Cu}^{2+}$ ,  $\tilde{K}_{j,\text{Cu}}$ , the ion-specific non-ideality parameters of the site  $j$  for  $\text{H}^+$  and  $\text{Cu}^{2+}$ ,  $n_{j,\text{H}}$ ,  $n_{j,\text{Cu}}$ , and the heterogeneity parameters of the site  $j$ ,  $p_j$ , which correspond to the reciprocal of the width of the affinity distribution, were optimized by fitting to the  $\text{Cu}^{2+}$  binding isotherms, while  $n_{j,\text{H}} \times p_j$  was kept equal to  $m_j$ .<sup>11</sup> The lower and upper boundaries were set to 0 and 1 for the  $m_j$ ,  $n_{j,i}$  and  $p_j$  parameters.

#### 2.4. XAS analysis

Copper K-edge XANES and extended X-ray absorption fine structure (EXAFS) analyses of  $\text{Cu}^{2+}$  reacted with HHA and PAHA were carried out at the BL-27B in the KEK Photon Factory (Tsukuba, Japan). The HA samples were dissolved in alkaline solutions at  $4.0 \text{ g L}^{-1}$  and stirred overnight under an Ar atmosphere. After adjusting the pH to 4 or 7 with 0.1 or 0.01 M HCl and NaOH, a 10 mM  $\text{CuCl}_2$  solution was added to achieve a  $\text{Cu}^{2+}$  loading of 80 mmol Cu per kg HA, and pH was re-adjusted to the original values. These values correspond to the  $\text{Cu}^{2+}$  binding amounts of 13.3 ( $\log[\text{Cu}^{2+}]_{\text{bound}} = -1.88$ ) and 310 ( $\log[\text{Cu}^{2+}]_{\text{bound}} = -0.51$ ) mmol  $\text{kg}^{-1}$ , respectively, according to the NICA-Donnan model calculation with the optimized parameters for HHA. After equilibration for two days, the samples were freeze-dried, mixed with boron nitride (BN), and pressed into pellets, which were covered by a Kapton® tape. Reference solid compounds ( $\text{Cu}^{\text{II}}\text{O}$ ,  $\text{Cu}^{\text{II}}\text{Cl}_2$ ,  $\text{Cu}^{\text{I}}\text{Cl}$ , and  $\text{Cu}^{\text{I}}\text{SCN}$ ) were dispersed in BN and pressed into pellets. In addition a 0.02 M  $\text{Cu}^{2+}$  solution with 0.04 M  $\text{L}(+)\text{-tartrate}$  at pH 7 was also measured as a reference.

Copper K-edge X-ray absorption spectra (XAS) were measured in fluorescence mode at 148 K using a liquid  $\text{N}_2$  cryostat equipped with Kapton® windows (CoolSpek, UNISOKU) for the HA samples and in transmission mode at room

temperature for the reference materials. A Si(111) double crystal monochromator was detuned by about 50% to reject higher harmonic intensity. Reduction and theoretical fitting of the obtained XAS data was performed by the Athena and Artemis software packages<sup>53</sup> and FEFF 6.<sup>54</sup> The details of the data reduction and fitting are given in the ESI.†

## 3. Results and discussion

### 3.1. Physicochemical properties of the HHSS

The elemental compositions and  $^{13}\text{C}$  NMR distributions of HHA and HFA are given in Table 1 and the more detailed physicochemical properties of HHA and HFA are summarized in Table S1 in the ESI† together with those of the IHSS and JHSS HSs and PAHA. These standard or reference HSs are isolated from various surface environments, ranging from soils (EHA from the Elliot soil, IHA and IFA from the Inogashira volcanic ash soil, DHA and DFA from the Dando forest soil), peats (PHA from the Pahokee peat), oxidation products of lignite (Leonardite HA, LHA), rivers (SRHA and SRFA from the Suwannee River), and lakes (NHA and NFA from the Nordic lake and BFA from the Biwako lake). The elemental compositions of the HHSS are characterized by their low oxygen and ash contents and high hydrogen and sulfur contents, compared to HAs and FAs from surface environments. The relatively small O/C and large H/C ratios of the HHSS can be seen in the van Krevelen plot (Fig. 1).<sup>55</sup> In Fig. S1 of the ESI† a similar plot with broader data from the literature is also shown. The locations of the standard and commercial surface HAs and FAs depend on their types and origins (Fig. 1). The former are characterized by relatively high O/C ratios; the latter exhibit a wide range of H/C ratios with constant and relatively small O/C ratios. The aquatic HA and FA are close to each other except for BFA. Groundwater HSs tend to have small O/C ratios, as is shown in Fig. S1.† Some groundwater HAs as well as marine HSs show relatively large H/C ratios. Compared with HSs from various environments, HHA and HFA are different in terms of the O/C and H/C ratios as is shown in Fig. 1. The large H/C values of the HHSS indicate the abundance of saturated carbons, which is in line with their small aromaticities estimated from the  $^{13}\text{C}$  NMR C distribution (Tables 1 and S1 in the ESI†). The highly aliphatic nature of organic matter in deep underground environments has been pointed out by several researchers.<sup>26,29,31</sup> Pettersson *et al.*<sup>26</sup> reported an even higher H/C value ( $\text{H/C} = 1.7$ ) for HA extracted from granitic groundwater at  $-280 \text{ m bgl}$ . Claret *et al.*<sup>31</sup> also reported the highly aliphatic nature of FAs extracted from argillite of Meuse and Opalinus shale and discussed their origin as oceanic sediments at high burial temperature.

The densities of oxygen-containing carboxylic and phenolic functional groups of the HHSS determined by conventional end-point acid–base titration in Table S1† are comparable to those of the surface HSs. This means that the oxygen depletion indicated by the small O/C ratios of the HHSS occurs in functional groups other than carboxylic and phenolic-type groups, as described by Thurman.<sup>56</sup> The UV/Vis optical properties of the HHSS are characterized by relatively small  $A_{250/210}$  and  $A_{350/280}$  ratios (Table S1†). This points to the presence of small



Table 1 Elemental compositions and  $^{13}\text{C}$  NMR carbon distributions of HHA and HFA

	Elemental composition <sup>a</sup> (%)						$^{13}\text{C}$ NMR <sup>b</sup> (%)				
	C	H	N	O	S	Ash	C <sub>I</sub>	C <sub>II</sub>	C <sub>III</sub>	C <sub>IV</sub>	C <sub>V</sub>
HHA	62.29	6.40	3.36	25.44	2.51	N.D. <sup>c</sup>	3.0	12.7	26.4	17.9	40.6
HFA	60.23	6.84	2.06	29.00	1.87	N.D. <sup>c</sup>	4.2	13.9	21.4	15.5	45.6

<sup>a</sup> Ash free basis. <sup>b</sup> C<sub>I</sub>: carbonyl C (190–220 ppm), C<sub>II</sub>: carboxyl C (165–190 ppm), C<sub>III</sub>: aromatic C (110–165 ppm), C<sub>IV</sub>: methoxyl and carbohydrate C (48–110 ppm), C<sub>V</sub>: aliphatic C (5–48 ppm). <sup>c</sup> Not detected.

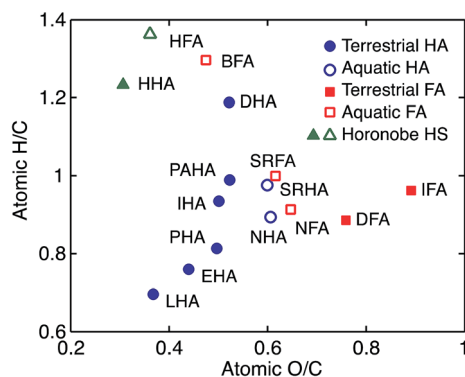


Fig. 1 van Krevelen plot of the HHSs, the IHSS and JHSS reference and standard HSs, and PAHA. The types of HS and origins are designated by different symbols and colors.

conjugated systems in the HHSs<sup>48</sup> and again in accordance with their low aromaticities.

The size distributions of the HHSs measured by FI-FFF are compared to those of the IHSS and JHSS standard HSs and PAHA in Fig. 2. For the surface HSs the sizes of the HAs are larger than those of the FAs. The size distributions of the HAs are largely overlapping, although their shapes are somewhat different from each other; EHA, IHA, and LHA possess multiple peaks. The size distributions of the FAs are all mono-modal, and the peak locations are different, depending on their sources. It seems that the JHSS FAs (BFA, DFA, and IFA) are somewhat smaller than the IHSS FAs (SRFA and NFA). The size distributions of HHA and HFA are mono-modal with the modal sizes of 0.6 and 0.3 nm, respectively, which are appreciably smaller than those of the surface HSs. Relatively small sizes of deep underground organic matter have been reported in the literature.<sup>57,58</sup> Bouby *et al.*<sup>58</sup> reported that organic matter in the Gorleben groundwater had a modal size of 1 nm. Saito *et al.*<sup>57</sup> compared the size distribution of organic matter in granitic and sedimentary groundwater by FI-FFF. The sedimentary groundwater was taken from a borehole at the same depth in the Horonobe URL as in this study and exhibited a mono-modal size distribution with a peak around 2 nm. This may indicate that HA and FA fractions may account for only a part of the dissolved organic matter in this groundwater.

The EAC of a HS corresponds to the number of electrons transferred to the HS from the mediator, normalized by the mass of the HS, and represents its redox capacity. For the HHSs, the EAC values are relatively small compared with those of the

IHSS and JHSS HSs (Fig. S2 in the ESI<sup>†</sup>). As in Aeschbacher *et al.*,<sup>49</sup> we found a linear relationship between the EAC and the aromaticities of the HSs investigated (Fig. S2<sup>†</sup>). This is because the concentration of quinone moieties, that are predominantly responsible for redox reactions in HSs, tends to be proportional to the amount of aromatic carbon.<sup>42</sup> Thus, the HHSSs with low aromaticities have small redox capacities compared with the surface HSs.

In summary the HHSs can be viewed as relatively small organic matter with abundant aliphatic carbons and sulfurs. The densities of acidic functional groups are comparable to those of the surface HSs. The differences between HHA and HFA are small. The cluster analysis (Fig. S3 in the ESI<sup>†</sup>) performed for the physicochemical properties compiled in Table S1<sup>†</sup> clearly indicates that they are different from the IHSS and JHSS HSs. BFA is an exception, being clustered into the same group as the HHSs. This may indicate the presence of similar formation processes among them.

### 3.2. H<sup>+</sup> and Cu<sup>2+</sup> binding isotherms to the HHSs

The charge/pH curves of HHA and HFA at different salt levels are presented in Fig. 3. The negative charge ( $-q$ ) of the HHSs increases with pH and salt concentration, as is usually seen for surface HSs.<sup>17</sup> The maximum negative charge of HFA is larger

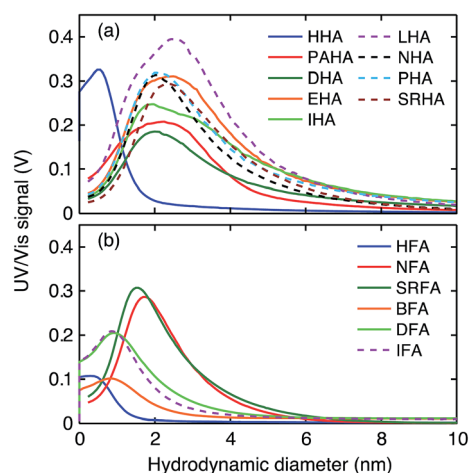


Fig. 2 Fractograms of the HHSs, the IHSS and JHSS reference or standard HSs, and PAHA by FI-FFF, using 5 mM Tris buffer as effluent. Fractionated HSs were measured by a UV/Vis detector at 255 nm. The fractograms of HAs are shown in (a) and those of FAs in (b).



than that of HHA, which predominantly arises from greater deprotonation at acidic pH ( $\text{pH} < 6$ ). This further suggests that HFA possesses more acidic functional groups, mostly carboxylic groups, than HHA. In Fig. 3 the charge/pH curves of the HHSSs are compared to those calculated by the NICA-Donnan model with the generic parameters derived for surface HSs (Table 2). At acidic pH the slopes of the curves are larger for the HHSSs. At neutral and alkaline pH this trend is reversed, although the differences are small. The slope of a charge/pH curve of a HS reflects the width of the corresponding affinity distribution of its functional groups. A smaller slope means a wider distribution and larger chemical heterogeneity.<sup>9</sup> Note that at  $6 < \text{pH} < 9$  the negative charges of the HHSSs hardly change, indicating that the number of the acidic functional groups having corresponding  $\text{pK}_a$  is small. Thus, these comparisons imply that the negative charges of the HHSSs largely originate from  $\text{H}^+$  dissociation from chemically homogeneous low-affinity sites, which should mainly consist of carboxylic groups located on the aliphatic chains of the HHSSs, considering their elemental compositions and  $^{13}\text{C}$ -NMR carbon distributions (Table 1). The salt dependence of the charge/pH curves is also different between the HHSSs and the model calculation. Relatively large salt effects are observed at neutral to alkaline pH for the HHSSs, but at acidic pH in the model calculation with the generic parameters.

The  $\text{Cu}^{2+}$  binding isotherms to HHA and HFA are presented in Fig. 4. The isotherms are similar between them. The binding amounts of  $\text{Cu}^{2+}$  to the HHSSs increases with the  $\text{Cu}^{2+}$

Table 2 Optimized NICA-Donnan parameters for  $\text{H}^+$  and  $\text{Cu}^{2+}$  binding to HHA and HFA. For comparison the generic parameters for HA and FA, denoted as GHA and GFA, are given<sup>18</sup>

	HHA	HFA	GHA	GFA
$q_0$ (eq $\text{kg}^{-1}$ )	-0.64	-0.53	—	—
$b$	0.81	0.87	0.49	0.57
$Q_{\text{max}1,\text{H}}$ (eq $\text{kg}^{-1}$ )	4.38	5.64	3.15	5.88
$p_1$	<i>1<sup>a</sup></i>	<i>1<sup>a</sup></i>	0.62	0.59
$Q_{\text{max}2,\text{H}}$ (eq $\text{kg}^{-1}$ )	4.44	4.09	2.55	1.86
$p_2$	0.36	0.27	0.41	0.70
$\log \tilde{K}_{1,\text{H}}$	3.74	3.63	2.93	2.34
$n_{1,\text{H}}$	0.82	<i>1<sup>a</sup></i>	0.81	0.66
$\log \tilde{K}_{2,\text{H}}$	10.62	10.48	8.00	8.60
$n_{2,\text{H}}$	<i>1<sup>a</sup></i>	<i>1<sup>a</sup></i>	0.63	0.76
$\log \tilde{K}_{1,\text{Cu}}$	1.32	1.16	2.23	0.26
$n_{1,\text{Cu}}$	<i>1<sup>a</sup></i>	<i>1<sup>a</sup></i>	0.56	0.53
$\log K_{2,\text{Cu}}$	14.43	15.05	6.85	8.26
$n_{2,\text{Cu}}$	0.28	0.29	0.34	0.36
$R^2$ ( $\text{H}^+$ ) <sup>b</sup>	0.9970	0.9975	—	—
$R^2$ ( $\text{Cu}^{2+}$ ) <sup>b</sup>	0.9951	0.9876	—	—

<sup>a</sup> The values in italic are constrained in physically meaningful ranges of the corresponding parameters (see the text of the ESI for details). <sup>b</sup> The correlation coefficients of the fitting for  $\text{H}^+$  and  $\text{Cu}^{2+}$ .

concentration and pH, as is expected for metal binding to surface HSs.<sup>18,38</sup> The observed pH dependency of  $\text{Cu}^{2+}$  binding is the result of diminished  $\text{H}^+$  competition to the functional groups of the HHSSs with an increase of pH. The  $\text{Cu}^{2+}$  binding amounts also slightly decrease with an increase of salt concentration due to screening of the negative electrostatic potential of the HHSSs. In Fig. 4 the  $\text{Cu}^{2+}$  binding isotherms calculated by the NICA-Donnan model with the generic parameters given in Table 2 are presented for comparison. The binding amounts of  $\text{Cu}^{2+}$  to the HHSSs are smaller than those of the model calculations regardless of pH and salt concentration. Weak binding of europium is also reported for HA and FA extracted from groundwater collected at -495 to 550 m bgl through a surface borehole in the Horonobe URL.<sup>33</sup> At pH 4 the slopes of the isotherms to the HHSSs are close to 1 in the log-log plot, which are larger than those of the model calculations with the generic parameters at the same pH. Interestingly, the differences in the slopes became smaller at higher pH, and at pH 8 for HHA it becomes similar to the slope of the calculated  $\text{Cu}^{2+}$  isotherms. The slope of a metal-binding isotherm of HS in a log-log plot is determined by the combination of the chemical heterogeneity of sites and the ion-specific non-ideality such as stoichiometry of the binding.<sup>9</sup> The slope close to 1 in the isotherms of the HHSSs at pH 4 together with the relatively large slopes of their charge-pH curves at acidic pH (Fig. 3) indicate  $\text{Cu}^{2+}$  binding to relatively homogeneous sites *via* mono-dentate coordination. At higher pH it seems that the binding mode tends to shift to coordination with greater denticity such as bi-dentate coordination.

### 3.3. NICA-Donnan modeling

The results of the NICA-Donnan fitting to the  $\text{H}^+$  and  $\text{Cu}^{2+}$  isotherms to HHA and HFA are presented in Fig. 3 and 4 and the

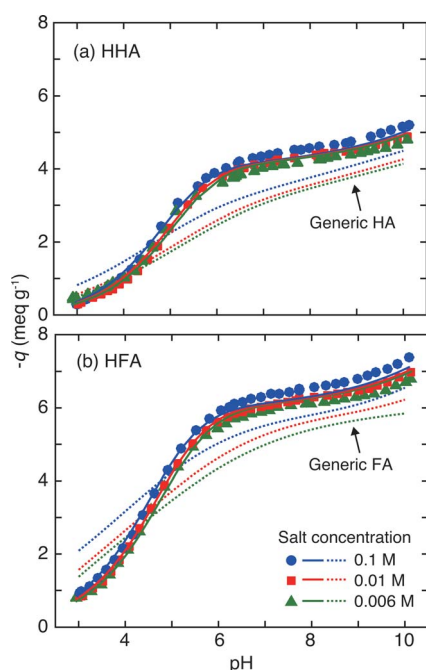


Fig. 3 Charge-pH curves (symbols) of HHA (a) and HFA (b) at the three salt concentrations. The solid curves represent the results of fitting to the NICA-Donnan model for the HHSSs and the dotted curves correspond to the calculation of the NICA-Donnan model with the generic parameters in Table 2.<sup>18</sup> The negative charges ( $-q$ ) are plotted in the ordinates.



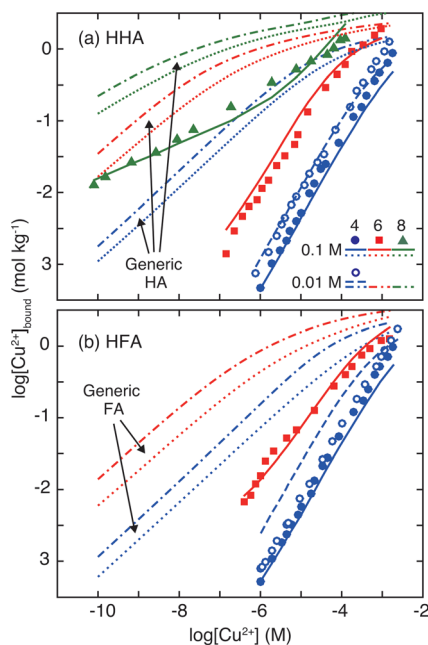


Fig. 4 Copper binding isotherms to HHA (a) at pH 4, 6, and 8 and to HFA (b) at pH 4 and 6, measured in the presence of 0.1 M NaClO<sub>4</sub>. For pH 4, the results with 0.01 M NaClO<sub>4</sub> are also presented. The solid and dashed curves correspond to the results of the NICA-Donnan fitting at 0.1 and 0.01 M NaClO<sub>4</sub>, respectively. The dotted and chained curves correspond to the calculation of the NICA-Donnan model with the generic parameters in Table 2 at 0.1 and 0.01 M salt concentrations.<sup>18</sup>

optimized parameters are given in Table 2 together with Milne's generic parameters.<sup>17</sup> The 95% confidence intervals and the correlation matrices of the optimized parameters are given in Tables S2–S4 in the ESI.† Note that some parameters associated with the high-affinity sites, namely  $Q_{\max 2, H}$ ,  $\log \tilde{K}_{2, H}$ , and  $\log \tilde{K}_{2, Cu}$  suffered from large errors. This is because that these parameters were not well fitted to the model due to the limited experimental conditions for H<sup>+</sup> and Cu<sup>2+</sup> binding to the HHSSs in alkaline pH (pH ≤ 10 for the charge–pH curves and pH ≤ 8 or 6 for the Cu<sup>2+</sup> isotherms). In order to unequivocally determine these parameters, potentiometric titration in non-aqueous media would be necessary.

For H<sup>+</sup> binding the model successfully reproduces the charge–pH curves, especially at pH < 6. At neutral to alkaline pH the model somewhat underestimated the magnitude of the salt effect. The electrostatic part of the NICA-Donnan model (eqn (S4) and (S5) in the ESI†) assumes a relatively simple functional form for the so-called Donnan volume, which depends only on the salt concentration.<sup>14</sup> Although the Donnan model is relatively simple with only one adjustable parameter and advantageous over other more sophisticated but complex models, its potential flaw for small FAs has been recognized.<sup>59</sup> Considering the sizes of HHA and HFA, which are smaller than the Debye length of the solutions (1 and 3 nm for 0.1 and 0.01 M NaClO<sub>4</sub>), electrostatic potential calculation by the rigid-sphere or ion-permeable sphere model would be more realistic.<sup>14</sup> The discrepancy observed at pH > 6 may also indicate the presence of a pH-dependent conformational change in the HHSSs. Such

conformational changes are common for linear aliphatic poly-electrolytes such as polymethacrylic acid.<sup>60</sup> For HHA, Cu<sup>2+</sup> binding is well reproduced by the model over a wide range of conditions, using the single set of the parameters. For HFA the model overestimated the salt effect and failed to describe the Cu<sup>2+</sup> binding at 0.01 M NaClO<sub>4</sub> and pH 4. It is likely that the model mishandles the electrostatic potential of HFA.

The optimized NICA-Donnan parameters for HHA and HFA are more or less similar to each other except for  $Q_{\max 1, H}$ , which is larger for HFA. The maximum densities of H<sup>+</sup> binding sites are similar between the high ( $j = 1$ ) and low ( $j = 2$ ) affinity sites in HHA. For HFA the density of the latter group was smaller by 1.5 meq g<sup>-1</sup>. The obtained parameters can be compared to those of surface HSSs with various origins and the generic parameters in Table 2.<sup>18</sup> The values of  $Q_{\max 1, H}$  of the HHSSs are in the ranges reported for the surface HSSs, while those of  $Q_{\max 2, H}$  are larger.<sup>17</sup> The median affinity constants of H<sup>+</sup> of the HHSs are larger than those of most of the surface HSSs and Milne's generic parameters. The heterogeneity parameter,  $p_j$ , and ion-specific non-ideality parameter,  $n_{j, H}$  are also relatively large for the HHSSs. This is especially the case for the low affinity carboxylic-type sites, reflecting the large slopes of their charge/pH curves (Fig. 3) at pH < 6. The Donnan parameters,  $b$ , are also larger for the HHSSs. Considering the large aliphaticity of the HHSSs as discussed in the physicochemical characterization, the  $\log \tilde{K}_{2, H}$  values of HHA (10.62) and HFA (10.48), which are larger than the corresponding values of the generic HA (8.60) and FA (8.00), may indicate a larger contribution of alcoholic hydroxyl groups to the sites of the HHSSs than those of surface HSSs, although the presence of phenolic groups with large pK<sub>a</sub> cannot be entirely neglected as the HHSSs still contain a certain amount of aromatic carbons (Table 1). This can also explain the weak H<sup>+</sup> buffering by the HHSSs at neutral to alkaline pH (Fig. 3).

The NICA-Donnan parameters of Cu<sup>2+</sup> binding to HHSSs are rather different from those of the generic parameters derived by Milne *et al.* (Table 1).<sup>18</sup> For the low-affinity sites  $\log \tilde{K}_{1, Cu}$  is larger for HHA and smaller for HFA than the corresponding generic parameters; whereas  $n_{1, H}$  for both HHA and HFA are 1 and larger than the corresponding generic parameters (0.56 for GHA and 0.53 for GFA). For the high-affinity sites  $\log \tilde{K}_{2, Cu}$  of HHA and HFA are larger than those of the generic parameters, and  $n_{2, H}$  are smaller. Thus, the Cu<sup>2+</sup> binding to the HHSSs are characterized by  $n_{1, Cu} = 1$  for the low-affinity sites and large  $\log \tilde{K}_{2, Cu}$  and small  $n_{2, Cu}$  values for the high-affinity sites. A ratio of the parameter  $n_{j, i}$  of a metal ion and proton is a good indicator of the underlying denticity of the complexation reaction ( $n_{i, j}/n_{j, H}$  close to 1 for mono dentate binding and 0.5 for bi-dentate binding). Thus, the optimized NICA-Donnan parameters for the HHSSs suggest the mono-dentate nature of Cu<sup>2+</sup> binding to the chemically homogeneous low-affinity sites at acidic pH. Considering the comparable or larger densities of the sites,  $Q_{\max 1, H}$ , of the HHSs to/than those of surface HSSs, this is most likely caused by sparsely distributed carboxylic groups on the aliphatic backbones of the HHSSs, with which it is hard to form bi-dentate coordination with Cu<sup>2+</sup>. This can also explain the weak Cu<sup>2+</sup> binding to the HHSSs (Fig. 4). The relatively small  $n_{2, Cu}/n_{2, H}$  values for the HHSSs together with the relatively small



$p_2$  values indicate that the more heterogeneous phenolic/alcoholic-type groups are involved in the binding of  $\text{Cu}^{2+}$  at neutral to alkaline pH *via* multi-dentate coordination. It is of interest to compare the NICA-Donnan parameters for the HHSs to those optimized for other groundwater HSSs. Marang *et al.*<sup>61</sup> reported the NICA-Donnan parameters for the binding of divalent and trivalent metal ions including  $\text{Cu}^{2+}$  to HA extracted from deep groundwater (−139 m bgl) of the Gorleben aquifer in Germany. The NICA-Donnan parameters of  $\text{Cu}^{2+}$  for this HA are more like those of GHA than those of HHA, suggesting a diversity of the ion binding properties of groundwater HSSs. Further research is needed to relate it to the origin and genesis of groundwater HSSs.

### 3.4. Oxidation state and chemical environment of $\text{Cu}^{2+}$ bound to HHA

The oxidation state of Cu and its coordination environment bound to HHA was assessed by XAS. The XANES spectra of  $\text{Cu}^{2+}$  bound to HHA and PAHA are compared to those of the reference compounds in Fig. 5. The  $\text{Cu}^{\text{I}}$  reference materials exhibit characteristic pre-edge features (8.985 keV for  $\text{CuSCN}$  and 8.988 keV for  $\text{CuCl}$ ) originating from  $1s \rightarrow 4p$  transitions.<sup>62</sup> The  $\text{Cu}^{\text{II}}$  compounds, on the other hand, are characterized by intense white lines around 8.997 to 9.000 keV due to  $1s \rightarrow$  continuum transitions.<sup>62</sup> The XANES spectra of  $\text{Cu}^{2+}$  bound to HHA and PAHA at pH 4 and 7 resemble those of  $\text{Cu}^{\text{II}}$  reference materials, especially Cu-tartrate. This suggests that reduction of  $\text{Cu}^{2+}$  bound to HHA and PAHA is negligible, although the magnified plot of the edge regions reveals a slight increase at 8.985 keV and a decrease at 8.998 keV for HHA (Fig. S4 in ESI†). Fulda *et al.*<sup>62</sup> reported reduction of  $\text{Cu}^{2+}$  upon binding to a soil HA under anoxic conditions by XAS. It has also been reported that SRFA rapidly reduces  $\text{Cu}^{2+}$  even under oxic conditions.<sup>63</sup> Virtually no reduction of  $\text{Cu}^{2+}$  by HHA may agree with its low EAC obtained by MER (Fig. S2†).<sup>49</sup>

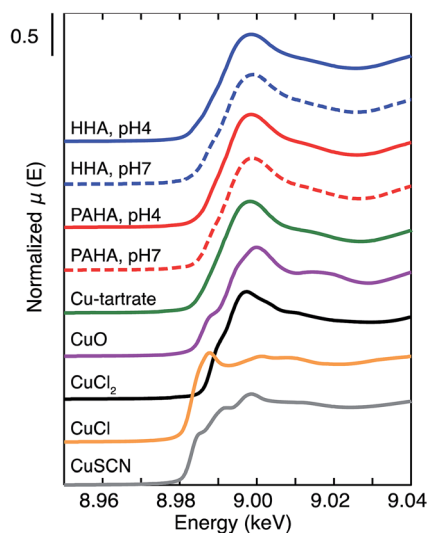


Fig. 5 XANES spectra of  $\text{Cu}^{2+}$  bound to HHA and PAHA at pH 4 and 7 together with those of the  $\text{Cu}^{\text{II}}$  and  $\text{Cu}^{\text{I}}$  reference materials.

The  $k^3$ -weighted EXAFS spectra of  $\text{Cu}^{2+}$  bound to HHA and PAHA at pH 4 and 7 (Fig. 6(a)) exhibit systematic differences between the two HAs at 5.7, 6.5, and 7.4  $\text{\AA}^{-1}$ . In Fig. S4 of the ESI† the same spectra are shown as an overlapped plot. The magnitudes of the corresponding Fourier transforms (Fig. 6(b) and S5(b) in the ESI†) are also different between them. For both HAs the Fourier transformed magnitudes are dominated by the intense peaks around 1.5  $\text{\AA}$ , which correspond to the scattering from the nearest O (and, to a lesser extent, N). For HHA additional peaks are noticeable around 2  $\text{\AA}$ , although their magnitudes are small. These peaks most likely originate from the Cu–S path as suggested by others.<sup>49,64</sup> This assignment agrees with the high S content of HHA (Table 1). Quantitative modeling of the first coordination sphere of  $\text{Cu}^{2+}$  (Fig. 5(b) and Table 3) shows that approximately four O exist at 1.93  $\text{\AA}$  for PAHA, which corresponds to the Jahn–Teller distorted coordination geometry around  $\text{Cu}^{2+}$ . For HHA at pH 4 the coordination number (CN) of O in the first shell is decreased and a small but non-negligible number of S (CN =  $0.4 \pm 0.2$ ) is found at 2.35  $\text{\AA}$ . At pH 7 the presence of S in the second shell is inconclusive. Note that this does not necessarily mean bi-dentate coordination of  $\text{Cu}^{2+}$  with O/N and S in HHA. Considering the results of the NICA-Donnan fitting (Fig. 4 and Table 2), it seems more likely that the two independent mono-dentate sites exist in HHA, as an EXAFS spectrum is a one-dimensional representation of the coexisting coordination environments of a target element. The S containing functional group could be the thioacetic group, R–COSH, which then should be a part of the low affinity sites in the NICA-Donnan modeling, as the  $pK_a$  value of thioacetic acid ( $\text{CH}_3\text{COSH}$ ,  $pK_a = 3.33$ ) is close to that of acetic acid ( $pK_a = 4.76$ ) and smaller than that of methanethiol ( $\text{CH}_3\text{SH}$ ,  $pK_a = 10.33$ ).<sup>65</sup> It is also noteworthy to mention that the contribution of S to  $\text{Cu}^{2+}$  binding to HHA might be underestimated, compared with that in the original groundwater, as the functional groups containing reduced S may be oxidized during the extraction and

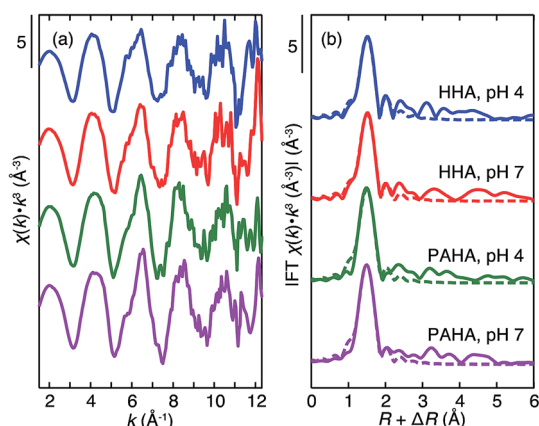


Fig. 6  $k^3$ -weighted Cu K-edge EXAFS spectra (a) and the corresponding Fourier transform magnitude (b) of  $\text{Cu}^{2+}$  bound to HHA and PAHA at pH 4 and 7. The  $\text{Cu}^{2+}$  loading was 80 mmol Cu per kg HA. Solid curves correspond to the experimental results and dashed curves in the Fourier transform magnitude plots to the results of theoretical fitting of the first coordination sphere of  $\text{Cu}^{2+}$  (see the text for the details).



Table 3 EXAFS parameters optimized for the first coordination sphere of Cu<sup>2+</sup> bound to HHA and PAHA at pH 4 and 7

	First shell (Cu–O/N)			Second shell (Cu–S)			$\Delta E_0$ (eV)
	R (Å)	CN <sup>a</sup>	$\sigma^{2b}$ (10 <sup>3</sup> Å <sup>2</sup> )	R (Å)	CN	$\sigma^{2b}$ (10 <sup>3</sup> Å <sup>2</sup> )	
<b>HHA</b>							
pH 4	1.95 ± 0.01	2.7 ± 0.6	3 ± 1	2.35 ± 0.04	0.4 ± 0.2	3 ± 1	1.53 ± 2.36
pH 7	1.95 ± 0.02	3.1 ± 0.9	4 ± 3	2.35 ± 0.16	0.1 ± 0.3	4 ± 3	1.52 ± 3.51
<b>PAHA</b>							
pH 4	1.94 ± 0.01	3.7 ± 0.8	5 ± 2	—	—	—	0.71 ± 2.80
pH 7	1.93 ± 0.01	3.6 ± 0.5	4 ± 1	—	—	—	1.19 ± 2.07

<sup>a</sup> Coordination number. <sup>b</sup> Debye–Waller factor. The Debye–Waller factor of the Cu–S shell was set to be equal to that of the Cu–O/H shell.

storage. For more detailed discussion, S speciation in the HHSs should be determined by soft X-ray absorption spectroscopy.<sup>23</sup>

## 4. Conclusion

The present study aims to reveal physicochemical and ion binding properties of the HHSs isolated from deep groundwater in a sedimentary rock formation. It is found that the HHSs are rather different from surface HSs, characterized by high aliphaticity and S contents and relatively small sizes. Proton and Cu<sup>2+</sup> binding was studied by potentiometric titration and fit to the NICA-Donnan model for comparison to their binding to surface HSs. The results clearly indicate distinctive binding behaviors of H<sup>+</sup> and Cu<sup>2+</sup> to the HHSs, likely caused by the unique chemical nature of their functional groups compared with those of surface HSs. These ions predominantly bind to chemically homogeneous carboxylic groups of the HHSs and to a lesser extent S containing groups by mono-dentate coordination at low pH, which can explain the larger slopes of their isotherms and the smaller magnitude of Cu<sup>2+</sup> binding than those of surface HSs. At neutral to alkaline pH H<sup>+</sup> dissociation from the HHSs is small, likely because the majority of the high affinity sites consist of alcoholic OH groups with larger pK<sub>a</sub>. At the same pH range the slope of the Cu<sup>2+</sup> isotherm to HHA becomes smaller and is close to the model calculations with the generic parameters, suggesting that the binding mode could change to bi-dentate coordination with both carboxylic and alcoholic/phenolic groups. The XAS analyses further indicate that Cu<sup>2+</sup> binds to HHA largely as Cu<sup>II</sup> via O/N containing functional groups and to a lesser extent S containing functional groups. The generality of the results obtained in this study should be examined in the future by performing similar investigations for HSs isolated from various groundwater samples and generic parameter sets applicable for groundwater HSs should be developed. The effects of co-existing metal ions, which are present in deep underground water at relatively high concentrations, on ion binding to the HHSs are of great interest as they can alter the electrostatic properties and secondary structures of the HHSs.

## Acknowledgements

The authors (T. S.) would like to thank Mr Lukman Steven for his assistance in the potentiometric titration and Dr Masayuki

Watanabe for the UV/Vis measurements. This research was partly supported by the Ministry of Economy, Trade and Industry (METI), Japan, and “Grant-in-Aid for Young Scientists (B)” (Grant No. 25820446), the Japan Society for the Promotion of Science. This work was carried out under the approval of the KEK-PF (2012G723 and 2012G527).

## References

- G. R. Aiken, D. M. McKnight, R. L. Wershaw and P. MacCarthy, *Humic Substances in Soil, Sediment and Water*, Wiley, New York, 1985.
- C. Baduel, M. E. Monge, D. Voisin, J. L. Jaffrezo, C. George, I. El Haddad, N. Marchand and B. D'Anna, *Environ. Sci. Technol.*, 2011, **45**, 5238–5244.
- F. J. Stevenson, in *Humic Substances in Soil, Sediments and Water*, ed. G. R. Aiken, D. M. McKnight, R. L. Wershaw and P. MacCarthy, John Wiley & Sons, New York, 1985, pp. 13–52.
- A. M. Jones, R. N. Collins, J. Rose and T. D. Waite, *Geochim. Cosmochim. Acta*, 2009, **73**, 4409–4422.
- J. Jiang and A. Kappler, *Environ. Sci. Technol.*, 2008, **42**, 3563–3569.
- G. Bronner and K. U. Goss, *Environ. Sci. Technol.*, 2011, **45**, 1307–1312.
- J. Buffle, *Complexation Reactions in Aquatic Systems: An Analytical Approach*, Ellis Horwood, Chichester, 1985.
- E. Tipping, *Cation binding by humic substances*, Cambridge University Press, Cambridge, 2002.
- L. K. Koopal, T. Saito, J. P. Pinheiro and W. H. van Riemsdijk, *Colloids Surf., A*, 2005, **265**, 40–54.
- J. F. McCarthy and J. M. Zachara, *Environ. Sci. Technol.*, 1989, **23**, 496–502.
- D. G. Kinniburgh, W. H. van Riemsdijk, L. K. Koopal, M. Borkovec, M. F. Benedetti and M. J. Avena, *Colloids Surf., A*, 1999, **151**, 147–166.
- E. Tipping, *Aquat. Geochem.*, 1998, **4**, 3–48.
- J. A. Marinsky and J. H. Ephraim, *Environ. Sci. Technol.*, 1986, **20**, 349–354.
- T. Saito, S. Nagasaki, S. Tanaka and L. K. Koopal, *Colloids Surf., A*, 2005, **265**, 104–113.
- G. S. Manning, *J. Phys. Chem.*, 1969, **51**, 924–934.
- E. Tipping, S. Lofts and J. E. Sonke, *Environ. Chem.*, 2011, **8**, 225–235.



- 17 C. J. Milne, D. G. Kinniburgh and E. Tipping, *Environ. Sci. Technol.*, 2001, **35**, 2049–2059.
- 18 C. J. Milne, D. G. Kinniburgh, W. H. van Riemsdijk and E. Tipping, *Environ. Sci. Technol.*, 2003, **37**, 958–971.
- 19 I. A. M. Ahmed, J. H. Taylor, M. Bieroza, H. Zhang and W. Davison, *Water Res.*, 2014, **67**, 276–291.
- 20 J. Xiong, L. K. Koopal, W. F. Tan, L. C. Fang, M. X. Wang, W. Zhao, F. Liu, J. Zhang and L. P. Weng, *Environ. Sci. Technol.*, 2013, **47**, 11634–11642.
- 21 K. Kovács, A. Gáspár, C. Sajgó, P. Schmitt-Kopplin and E. Tombácz, *Geochem. J.*, 2012, **46**, 211–224.
- 22 K. Longnecker and E. B. Kujawinski, *Geochim. Cosmochim. Acta*, 2011, **75**, 2752–2761.
- 23 T. Schäfer, G. Buckau, R. Artinger, J. I. Kim, S. Geyer, M. Wolf, W. F. Bleam, S. Wirick and C. Jacobsen, *Org. Geochem.*, 2005, **36**, 567–582.
- 24 R. Artinger, G. Buckau, S. Geyer, P. Fritz, M. Wolf and J. I. Kim, *Appl. Geochem.*, 2000, **15**, 97–116.
- 25 C. Gron, L. Wassenaar and M. Krog, *Environ. Int.*, 1996, **22**, 519–534.
- 26 C. Pettersson, J. Ephraim and B. Allard, *Org. Geochem.*, 1994, **21**, 443–451.
- 27 A. Courdouan, I. Christl, S. Meylan, P. Wersin and R. Kretschmar, *Appl. Geochem.*, 2007, **22**, 1537–1548.
- 28 A. Courdouan, I. Christl, S. Meylan, P. Wersin and R. Kretschmar, *Appl. Geochem.*, 2007, **22**, 2926–2939.
- 29 L. Gasset, J. Brevet, T. Schafer, F. Claret, E. C. Gaucher, A. Albrecht and A. Ambles, *Org. Geochem.*, 2010, **41**, 221–233.
- 30 A. Courdouan, I. Christl, T. Rabung, P. Wersin and R. Kretschmar, *Environ. Sci. Technol.*, 2008, **42**, 5985–5991.
- 31 F. Claret, T. Schafer, T. Rabung, M. Wolf, A. Bauer and G. Buckau, *Appl. Geochem.*, 2005, **20**, 1158–1168.
- 32 J. J. Alberts, Z. Filip and N. Hertkorn, *J. Contam. Hydrol.*, 1992, **11**, 317–330.
- 33 M. Terashima, S. Nagao, T. Iwatsuki, N. Fujitake, Y. Seida, K. Iijima and H. Yoshikawa, *J. Nucl. Sci. Technol.*, 2012, **49**, 804–815.
- 34 T. Iwatsuki, R. Furue, H. Mie, S. Ioka and T. Mizuno, *Appl. Geochem.*, 2005, **20**, 2283–2302.
- 35 K. Hama, T. Kunimaru, R. Metcalfe and J. Martin, *Phys. Chem. Earth*, 2007, **32**, 170–180.
- 36 S. Kurosawa, S. C. James, M. Yui and M. Ibaraki, *J. Colloid Interface Sci.*, 2006, **298**, 467–475.
- 37 Y. Tachi, K. Yotsuji, Y. Seida and M. Yui, *Geochim. Cosmochim. Acta*, 2011, **75**, 6742–6759.
- 38 T. Saito, S. Nagasaki, S. Tanaka and L. K. Koopal, *Radiochim. Acta*, 2004, **92**, 567–574.
- 39 J. W. J. van Schaik, D. B. Kleja and J. P. Gustafsson, *Geochim. Cosmochim. Acta*, 2010, **74**, 1391–1406.
- 40 L. M. Gaetke and C. K. Chow, *Toxicology*, 2003, **189**, 147–163.
- 41 J. T. Rubino and K. J. Franz, *J. Inorg. Biochem.*, 2012, **107**, 129–143.
- 42 H. Kurikami, R. Takeuchi and S. Yabuuchi, *Phys. Chem. Earth*, 2008, **33**, S37–S44.
- 43 R. S. Swift, in *Methods of soil analysis. Part 3-chemical methods*, ed. D. L. Sparks, A. L. Page, P. A. Helmke, R. H. Loeppert, P. Soltanpour, M. A. Tabatabai, C. Johnston and M. E. Sumner, Soil Science Society of America, Madison, 1996, p. 1011.
- 44 M. A. Wilson, *Eur. J. Soil Sci.*, 1981, **32**, 167–187.
- 45 N. Fujitake and M. Kawahigashi, *Soil Sci. Plant Nutr.*, 1999, **45**, 359–366.
- 46 T. Saito, L. K. Koopal, W. H. van Riemsdijk, S. Nagasaki and S. Tanaka, *Langmuir*, 2004, **20**, 689–700.
- 47 F. J. Stevenson, *Humus Chemistry*, John Wiley & Sons, New York, 1982.
- 48 S. Lukman, T. Saito, N. Aoyagi, T. Kimura and S. Nagasaki, *Geochim. Cosmochim. Acta*, 2012, **88**, 199–215.
- 49 M. Aeschbacher, M. Sander and R. P. Schwarzenbach, *Environ. Sci. Technol.*, 2010, **44**, 87–93.
- 50 D. G. Kinniburgh, C. J. Milne and P. Venema, *Soil Sci. Soc. Am. J.*, 1995, **59**, 417–422.
- 51 C. J. Milne, D. G. Kinniburgh, J. C. M. de Wit, W. H. van Riemsdijk and L. K. Koopal, *J. Colloid Interface Sci.*, 1995, **175**, 448–460.
- 52 W. L. Lindsay, *Chemical equilibria in soils*, John Wiley & Sons, New York, 1979.
- 53 B. Ravel and M. Newville, *J. Synchrotron Radiat.*, 2005, **12**, 537–541.
- 54 S. I. Zabinsky, J. J. Rehr, A. Ankudinov, R. C. Albers and M. J. Eller, *Phys. Rev. B: Condens. Matter Mater. Phys.*, 1995, **52**, 2995–3009.
- 55 J. A. Rice and P. MacCarthy, *Org. Geochem.*, 1991, **17**, 635–648.
- 56 E. M. Thurman, in *Humic Substances in Soil, Sediments and Water*, ed. G. R. Aiken, D. M. Mcknight, R. L. Wershaw and P. MacCarthy, John Wiley & Sons, New York, 1985.
- 57 T. Saito, T. Hamamoto, T. Mizuno, T. Iwatsuki and S. Tanaka, *J. Anal. At. Spectrom.*, 2015, **30**, 1229–1236.
- 58 M. Bouby, N. Finck and H. Geckeis, *Mineral. Mag.*, 2012, **76**, 2709–2721.
- 59 M. F. Benedetti, W. H. van Riemsdijk and L. K. Koopal, *Environ. Sci. Technol.*, 1996, **30**, 1805–1813.
- 60 R. D. Porasso, J. C. Benegas and M. A. G. T. van den Hoop, *J. Phys. Chem. B*, 1999, **103**, 2361–2365.
- 61 L. Marang, P. E. Reiller, S. Eidner, M. U. Kumke and M. F. Benedetti, *Environ. Sci. Technol.*, 2008, **42**, 5094–5098.
- 62 B. Fulda, A. Voegelin, F. Maurer, I. Christl and R. Kretschmar, *Environ. Sci. Technol.*, 2013, **47**, 10903–10911.
- 63 A. N. Pham, A. L. Rose and T. D. Waite, *J. Phys. Chem. A*, 2012, **116**, 6590–6599.
- 64 A. Manceau and A. Matynia, *Geochim. Cosmochim. Acta*, 2010, **74**, 2556–2580.
- 65 *CRC Handbook of Chemistry and Physics*, ed. D. R. Lide, Taylor & Francis, Boca Raton, 2005.

